GEOLOGICAL JOURNAL
Geol. J. **37**: 167–186 (2002)
Published online in Wiley InterScience (www.interscience.wiley.com). DOI: 10.1002/gj.907

Geochemical and Nd-Sr-Pb isotopic evidence on the origin and geodynamic evolution of mid-Cretaceous continental arc volcanic rocks of the Spences Bridge Group, south-central British Columbia

ALAN D. SMITH[1] and DEREK THORKELSON[2]*

[1]*Centro de Investigación en Energía, Universidad Nacíonal Autónoma de México, Temixco, Morelos, México*
[2]*Department of Earth Sciences, Simon Fraser University, Burnaby, British Columbia, Canada*

The mid-Cretaceous Spences Bridge Group (SBG) comprises a series of basaltic to rhyolitic lavas and related volcaniclastic rocks (Pimainus Formation) overlain by a succession of mainly amygdaloidal andesites (Spius Formation) related to the closure of the Methow–Tyaughton basin and accretion of the Insular terrane in the North American Cordillera. Geochemical variation in the SBG is related primarily to metasomatic processes in the mantle wedge. Pimainus lavas include low- to high-K, tholeiitic and calc-alkaline types, and have isotopic compositions ($\varepsilon_{Nd}(100Ma) = +5.2$ to $+7.0$, $\varepsilon_{Sr}(100Ma) = -10$ to -20, $^{206}Pb/^{204}Pb = 18.82$ to 18.91, $^{207}Pb/^{204}Pb = 15.55$ to 15.60, $^{208}Pb/^{204}Pb = 38.24$ to 38.43) between the ranges for primitive arcs and accreted terrane crust. Crustal sources are identified only for some low–medium K dacite and rhyolite compositions. The occurrence of intermediate compositions with high MgO contents (up to 6 wt%) and the presence of adakitic trace element features in medium–high K felsic lavas attests to metasomatism of the mantle wedge by slab melts during Pimainus volcanism. Spius lavas have comparable K_2O and Pb isotopic compositions to the Pimainus, even higher MgO (up to 9.2 wt%), and display a mild intraplate character in having up to 0.6 wt% P_2O_5, 15 ppm Nb, and 240 ppm Zr. Spius Nd – Sr isotopic compositions ($\varepsilon_{Nd}(100Ma) = +5.3$ to $+6.9$, $\varepsilon_{Sr}(100Ma) = -14$ to -25) define an array extending from Pimainus to alkaline seamount compositions. The low ε_{Sr} values, elevated high field strength element contents, and moderate silica contents suggest Spius volcanism was related to the introduction of small melt fractions from the asthenosphere into the mantle wedge which had previously generated Pimainus melts. The range of compositional types in the Pimainus Formation constrains tectonic scenarios to include an elevated slab thermal regime, likely from approach of an ocean ridge system toward the continental margin. Spius volcanism may have been generated by asthenospheric upwelling triggered by slab window development or slab-hinge roll-back on closure of the Methow–Tyaughton basin. Copyright © 2002 John Wiley & Sons, Ltd.

Received 14 September 2000; revised version received 8 September 2001; accepted 2 October 2001

KEY WORDS arcs; North American Cordillera; Cretaceous; adakites; intraplate signatures

1. INTRODUCTION

The Spences Bridge Group (SBG) is a succession of mid-Cretaceous continental arc volcanic and sedimentary rocks exposed in a 215 × 25 km belt along the western edge of the Intermontane terranes of the North American Cordillera (Figure 1). Correlation of the SBG with the Kasalka and Skeena volcanics farther north in British Columbia suggests that the SBG belonged to part of an extensive late Mesozoic continental arc (Thorkelson and Rouse 1989; Souther 1991). The location and timing of volcanism implies that the arc was related to closure of a marginal basin whose remnants are preserved in terranes of the Early to Middle Mesozoic Methow–Tyaughton trough. The middle Cretaceous strata of the Methow–Tyaughton succession appear to represent a fore-arc assemblage related to SBG volcanism, although facies transitions and stratigraphic linkages with the SBG have not been clearly demonstrated. Early Late Cretaceous closure of the Methow–Tyaughton basin appears to be broadly

* Correspondence to: Alan D. Smith, Centro de Investigación en Energía, Universidad Nacíonal Autónoma de México, Apartado Postal 34, Temixco, Morelos 62580, México. E-mail: muic2000@yahoo.com

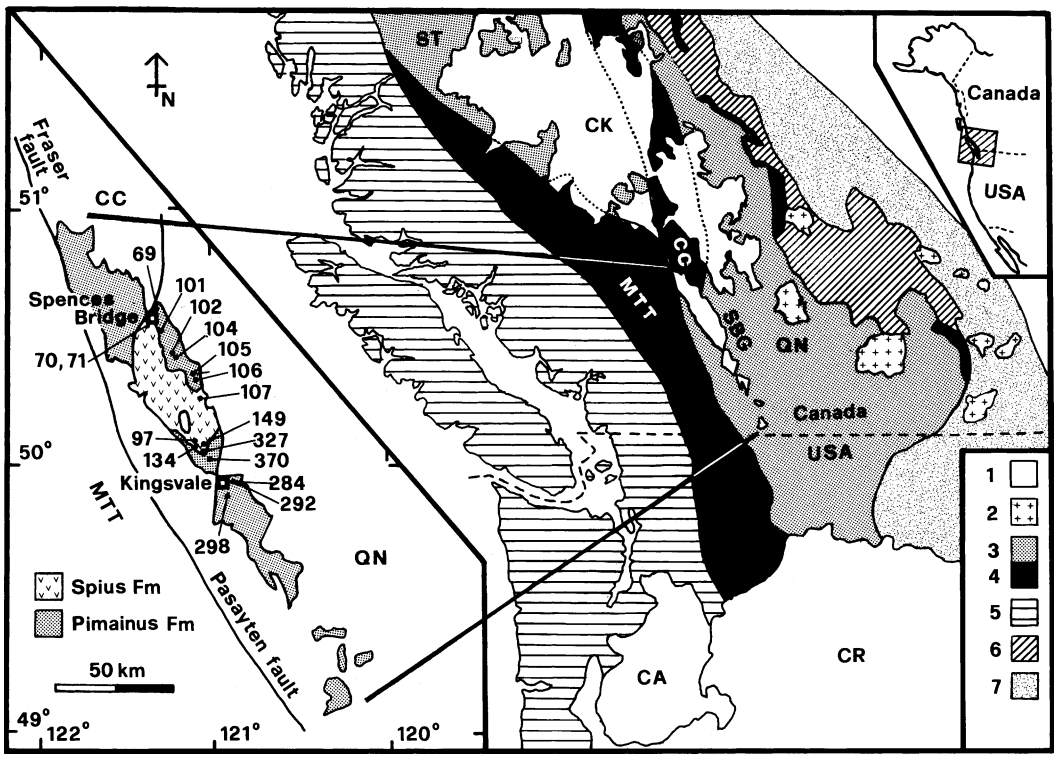

Figure 1. Location of the Spences Bridge arc (SBG) in southern British Columbia relative to: 1, volcanic provinces (CA, northern Cascades; CK, Chilcotin-Kamloops; CR, Columbia River); 2, Cretaceous granitoids; 3, accreted arc terranes of the Intermontane belt (QN, Quesnel terrane; ST, Stikine terrane); 4, ocean floor terranes (CC, Cache Creek terrane; MTT, terranes of the Methow–Tyaughton trough), 5, Insular terrane; 6, continental margin terranes (Kootenay, Barkerville, Monashee); 7, Purcell–Windermere sediments. Inset: sample locations within the SBG (boundaries as suggested by Monger and Berg 1987; Thorkelson and Rouse 1989).

synchronous with open folding of the SBG into a broad synclinorium, contraction in the Coast Belt, and collision of the Insular terrane with the previously accreted terranes of the Intermontane Belt (Duffell and McTaggart 1952; Thorkelson and Smith 1989; Souther 1991; Journeay and Friedman 1993). The age of oceanic crust preserved in the Methow–Tyaughton basin has been inferred from small relics to be of Jurassic or Triassic age (Ray 1986; Smith 1993), but the age of crust subducted during generation of the SBG has not been constrained. Inferences about events during basin closure may, however, be drawn from the geochemistry of the arc volcanism, and while the SBG displays many typical features of arc rocks, the appearance of mild intraplate signatures characterized by elevated abundances of high field strength elements (HFSE) in andesitic compositions toward the top of the volcanic succession (Thorkelson and Smith 1989) has considerable implications for the processes within the arc.

In modern arcs, HFSE-enriched lavas may be found toward the back-arc region, in rifting environments, and where the subducting slab is characterized by an elevated thermal regime (Pearce 1982; Gill and Whelan 1989). The signatures found toward the back-arc region, as in the example of the Cascade arc, may result from melting in the mantle wedge when amphibole, which concentrates HFSE, ceases to be a residual phase (Borg *et al.* 1997). Alternatively, declining fluid inputs from the slab toward the back-arc region, may allow melting of pre-existing low melting point components in the mantle wedge (Leeman *et al.* 1990). Enrichments in HFSE during advanced stages of rifting, as in the Fiji arc (Gill and Whelan 1989), and during the development of slab windows (Hole *et al.* 1991, 1995; Johnston and Thorkelson 1997), are imparted from asthenospheric sources. Elevated thermal regimes in arcs are usually associated with the subduction of young oceanic crust, and may result in either early dehydration of the slab allowing tapping of mantle less affected by metasomatism (Harry and Green 1999), or

melting of the subducting slab (Defant and Kepezhinskas 2001). Adakites are typically associated with slab melting (Kay 1978; Defant and Drummond 1990), although Nb-enriched arc basalts have also been suggested to be the product of metasomatization of the mantle wedge by small melt fractions from the slab (Sajona *et al.* 2000; Defant and Kepezhinskas 2001). The narrow width of the Spences Bridge arc limits the applicability of models involving cross-strike variations in source composition; however, scenarios involving elevation of the slab thermal regime are a consideration from the association of the SBG with basin closure and the possibility of a spreading ridge system approaching the continental margin. The geochemical features of the SBG are thus of relevance to both understanding arc processes and events during the last major episode of crustal growth in the Cordillera, and in this study new data are presented to identify the source components involved in the generation of the SBG and to refine models for the mid-Cretaceous tectonics of the region.

2. BACKGROUND AND SAMPLING

The main belt of the SBG lies south of the Fraser fault system, where the strata sit in a faulted synclinorium flanked mainly by older arc and ocean island assemblages of the Quesnel and Cache Creek terranes (Duffell and McTaggart 1952; Monger and McMillan 1984; Monger and Berg 1987). Rocks of the SBG have undergone little alteration, with metamorphism having reached only zeolite grade (Thorkelson and Rouse 1989). The stratigraphy was described by Thorkelson (1985) and Thorkelson and Rouse (1989) who divided the SBG into two units, the Pimainus and Spius Formations. The lower unit, the Pimainus Formation, comprises approximately equal proportions of basaltic to rhyolitic lavas intercalated with pyroclastic material and clastic sediments including fluvial sandstones and conglomerates, and has been considered to represent a stratovolcano succession (Thorkelson and Smith 1989). The upper unit, the Spius Formation, is a succession of homogeneous amygdaloidal andesites, scoria and tuff with little associated sediment. In contrast to the Pimainus Formation, which is distributed throughout the volcanic belt, the Spius Formation is restricted to a 50×20 km area in the centre of the belt, where it has been interpreted as a shield volcano sequence (Thorkelson and Smith 1989). Maximum thicknesses are up to 2.5 km for the Pimainus and 1 km for the Spius. Late Albian ages are indicated for both formations from leaf fossils, palynomorphs, and K-Ar and U-Pb dating (Thorkelson and Rouse 1989; Irving and Thorkelson 1990).

The mineralogy of the Pimainus lavas is dominated by a phenocryst suite of plagioclase and pyroxene, whereas many of the more mafic Spius lavas contain pseudomorphs of serpentine-after-olivine whose euhedral outlines imply surface equilibration with the melt (Thorkelson 1985). Some Spius acid andesites also contain olivine pseudomorphs, but others have been noted with Pimainus-like plagioclase and pyroxene crystals which are variably embayed and disintegrated suggesting derivation from an earlier, Pimainus-type melt. The importance of volatiles in controlling the mineralogy was stressed by Thorkelson (1985). Spius flows are more amygdaloidal than those of the Pimainus and probably contained a greater proportion of volatiles. As discussed by Kushiro (1975), such a feature could suppress the crystallization of plagioclase and pyroxenes while stabilizing olivine to shallow depth. Pimainus compositions may also have had a high initial volatile content, but the fractionation assemblage suggests this was lost during differentiation in shallow magma chambers. The implication of the mineralogy is that Spius lavas were erupted more rapidly, and hence were likely of higher temperature, and deeper origin than Pimainus types.

Samples were obtained from the central part of the SBG belt between the towns of Spences Bridge and Kingsvale (Figure 1). At localities near Kingsvale, studied in detail by Thorkelson (1985), the Spius Formation conformably and gradationally overlies the Pimainus. Similar relations are evident within a few kilometres of Spences Bridge, where lavas of the Spius Formation directly overlie, and possibly interfinger with those of the Pimainus. The gradational contacts may result from interdigitation of flows from separate eruptive centres, or result from variations in the supply of magma types to an individual volcano (Thorkelson and Smith 1989). Farther to the southwest between Spences Bridge and Kingsvale, lacustrine strata separate the formations and indicate a local hiatus in volcanic deposition. For the purposes of identifying the sources involved in magma genesis, the SBG samples have been classified according to formation on the basis of lithostratigraphy mapped at scales ranging

from 1:25 000 to 1:100 000. South of Spences Bridge, recent mapping and reinterpretations indicate the presence of domes and short flows of felsic lava within the Spius Formation that were previously assigned to the Pimainus Formation; hence the map pattern in Figure 1 differs somewhat from that shown on previous maps such as in Thorkelson and Rouse (1989).

3. ANALYTICAL PROCEDURES

Major and trace element analyses were performed by X-ray fluorescence spectroscopy (Table 1). Additionally, rare earth elements (REE) and selected trace elements were analysed by either conventional instrumental neutron activation analysis (INAA) or by the PIGS method of Smith *et al.* (1990) at the Ecole Polytechnique SLOWPOKE facility (Table 2). PIGS is a pre-irradiation group concentration method involving the analysis of the REE relative to Sm by neutron activation analysis from an aliquot removed during Sm-Nd chemical procedures. The REE content of the rock is then found by normalization to the Sm content of the rock determined by isotope dilution. As the method uses the same reactor and detector equipment, the results are directly comparable to REE analysed by conventional INAA. Nd and Sr isotopic analyses were performed using MM30 and MAT262 mass spectrometers at the University of Alberta and National Cheng Kung University laboratories following the method outlined in Smith *et al.* (1990) Table 3. Nd isotopic ratios were normalized to $^{146}Nd/^{144}Nd = 0.7219$, Sr isotopic ratios to $^{86}Sr/^{88}Sr = 0.1194$. Nd and Sr analyses are reported relative to $^{143}Nd/^{144}Nd = 0.511845$ and $^{87}Sr/^{86}Sr = 0.710240$ for the LaJolla and SRM987 standards, respectively. Chemistry for Pb followed conventional procedures involving HBr-extraction. Pb isotopic analyses were performed on a MM30 mass spectrometer at the University of Alberta with precision on each analysis typically $\pm 0.01\%$. Five replicate analyses of the SRM981 standard gave mean and two sigma standard error values of $^{206}Pb/^{204}Pb = 16.930 \pm 0.008$, $^{207}Pb/^{204}Pb = 15.486 \pm 0.010$,

Table 1. Major and trace element data for Spences Bridge Group volcanic rocks by X-ray fluorescence spectroscopy

	101F† P	101I P	101E P	102C P	370B† P	101C P	327C P	104B P	102D P	106 P	74B P	102G P	102E P	102F P
SiO_2	49.26	49.76	50.93	51.77	54.56	55.79	56.94	58.09	58.59	59.57	62.20	63.43	67.53	69.81
TiO_2	1.32	1.04	1.33	1.11	0.94	1.45	1.11	0.98	1.46	0.96	0.83	0.39	0.45	0.36
Al_2O_3	15.83	17.08	14.91	15.88	17.23	15.50	17.37	17.19	15.83	16.87	16.03	19.42	18.31	16.61
MnO	0.19	0.15	0.20	0.18	0.17	0.14	0.14	0.15	0.17	0.11	0.13	0.07	0.06	0.05
FeO*	10.22	9.08	8.66	9.28	8.36	9.21	8.12	7.01	7.84	6.22	6.02	2.00	2.68	1.90
MgO	9.29	9.99	6.27	7.65	6.06	4.92	4.00	5.02	4.68	4.11	3.70	1.75	0.58	1.32
CaO	9.47	10.04	11.33	8.44	9.55	7.60	8.39	6.76	6.33	6.81	6.00	5.90	4.11	3.30
Na_2O	3.51	2.54	4.53	2.96	2.24	2.85	2.36	3.10	3.62	3.71	2.76	4.11	4.01	4.14
K_2O	0.64	0.11	1.62	2.43	0.66	2.10	1.27	1.49	0.95	1.31	2.11	2.77	2.05	2.39
P_2O_5	0.31	0.20	0.22	0.29	0.22	0.43	0.30	0.20	0.51	0.35	0.20	0.12	0.21	0.12
Rb	16	6	27	44	6	34	38	20	16	24	35	54	37	47
Ba	289	144	1135	1376	252	529	387	503	685	597	644	770	627	800
Sr	580	616	875	595	786	642	666	671	413	591	519	406	286	374
Y	15	20	17	23	23	30	23	24	36	24	21	14	19	12
Nb	6	4	7	8	4	11	5	7	10	15	6	8	7	8
Zr	91	78	97	145	76	229	118	149	218	198	136	165	152	154
Ni	79	22	90	43	33	18	15	7	4	44	18	4	9	4
Cr	—	—	—	—	78	—	17	—	—	—	61	—	—	—
FeO*/MgO	1.10	0.91	1.38	1.21	1.38	1.87	2.03	1.40	1.67	1.51	1.63	1.14	4.62	1.44
$(Sr/P)_N$	1.93	3.18	4.10	2.12	3.68	1.54	2.29	3.46	0.84	1.74	2.68	3.49	1.40	3.22
K/Rb	332	152	499	459	914	513	278	619	493	454	501	426	460	423

Continues

Table 1. Continued

	298C P	105 P	71C S	134B† S	69C S	107 S	284C S	71D S	97B† S	292C S	149A S	70 S	71A S
SiO_2	73.79	75.04	52.98	53.85	54.10	54.78	56.34	57.02	57.94	59.70	60.54	60.80	69.79
TiO_2	0.34	0.27	1.26	1.17	1.64	0.96	1.35	1.32	1.20	1.03	0.97	1.62	0.55
Al_2O_3	15.19	14.35	15.48	17.81	15.75	16.27	17.05	17.12	18.03	16.84	16.28	15.21	15.66
MnO	0.06	0.07	0.18	0.14	0.17	0.16	0.16	0.22	0.14	0.10	0.12	0.16	0.08
FeO*	1.95	2.07	8.77	8.34	9.47	7.90	7.90	7.68	7.15	6.40	6.47	7.79	2.94
MgO	0.41	0.27	9.24	5.28	4.82	9.02	4.90	3.79	5.86	4.53	5.03	4.05	2.01
CaO	1.01	1.29	8.42	8.07	7.20	6.41	8.76	7.15	4.79	7.84	6.88	3.61	1.66
Na_2O	4.21	5.47	2.63	3.29	3.88	2.93	2.39	3.63	2.67	2.38	2.40	4.12	4.98
K_2O	2.94	1.07	0.61	1.45	2.53	1.26	0.61	1.72	1.71	0.76	0.98	2.03	3.13
P_2O_5	0.10	0.10	0.44	0.59	0.43	0.31	0.54	0.34	0.51	0.40	0.31	0.61	0.20
Rb	66	24	10	17	37	19	7	25	27	9	20	40	65
Ba	912	415	346	341	1233	543	549	660	530	577	348	701	726
Sr	284	60	760	732	794	690	803	709	527	772	780	534	453
Y	18	30	24	29	32	24	33	29	30	25	24	35	31
Nb	7	11	13	14	12	7	11	10	12	15	6	12	13
Zr	148	202	204	218	241	132	200	231	200	178	134	235	305
Ni	3	0	87	82	11	77	69	14	102	73	63	1	7
Cr	—	—	—	138	—	—	119	—	131	142	104	—	—
FeO*/MgO	4.76	7.67	0.95	1.58	1.96	0.88	1.61	2.03	1.22	1.41	1.29	1.92	1.46
$(Sr/P)_N$	2.93	0.62	1.78	1.28	1.90	2.30	1.53	2.15	1.07	1.99	2.60	0.90	2.34
K/Rb	370	370	507	709	568	551	724	572	526	702	407	422	400

Sample affiliation: P, Pimainus Formation; S, Spius Formation
Major elements have been recalculated to 100 weight % on a volatile-free basis. Trace elements in ppm.
*FeO total iron as FeO
†From Thorkelson and Smith (1989)
$(Sr/P)_N$ normalized to primitive mantle abundances of Sun and McDonough (1989) of 95 ppm P, 21.1 ppm Sr

$^{208}Pb/^{204}Pb = 36.696 \pm 0.020$. Blanks were typically < 400 pg Pb, < 250 pg Nd and < 1 ng Sr. Epsilon values were calculated using present-day $^{143}Nd/^{144}Nd = 0.512638$, $^{147}Sm/^{144}Nd = 0.1967$ and $^{87}Sr/^{86}Sr = 0.704780$, Rb/Sr = 0.031 for CHUR and Bulk Earth (BE), respectively.

4. RESULTS

4.1 Pimainus Formation

The Pimainus samples cover the range of composition (48 to 75 wt% SiO_2) from basalt through rhyolite. Iron enrichment is seen only in some basaltic and rhyolitic samples. Intermediate compositions have MgO contents up to 6 wt%, transitional between typical arc lavas and high-Mg andesites (Figure 2). FeO*/MgO ratios are between 0.9 and 2.0, and the samples define a trend crossing from the tholeiitic to calc-alkaline field on the FeO*/MgO versus silica diagram of Miyashiro (1974) (Figure 2). However, with Ni and Cr contents below 90 ppm and 205 ppm, respectively, the samples do not meet the criteria (FeO*/MgO < 1.0, > 200 ppm Ni, > 400 ppm Cr; Tatsumi and Eggins 1995) for primitive mantle-derived melts. Alkali contents are variable, with compositions ranging from low to high K in terms of K_2O–silica classification, although medium K-types predominate (Figure 2). Both tholeiitic and calc-alkaline fractionation trends dominated by olivine–plagioclase–magnetite and plagioclase–pyroxene, respectively, are seen in Ti–Zr variation (Figure 3). Regional variation is apparent in that samples from the north of the study area around Spences Bridge (notably samples 101E,F,I) fall within the arc

Table 2. Rare earth and selected trace elements (in ppm) by neutron activation methods

	101F P INAA	101I P INAA	101E P INAA	327C P INAA	102D P INAA	102F P INAA†	298C P PIGS	134B S INAA†	71C S INAA	284C S PIGS	71D S INAA	97B S PIGS	292C S PIGS	70 S INAA	149A S PIGS
La	9.55	8.51	10.7	11.7	22.1	15.9	17.9	29.0	16.5	31.9	18.6	35.3	23.6	21.0	18.1
Ce	20.0	16.5	21.0	26.7	44.7	26.8	32.8	59.9	34.9	67.1	38.2	65.8	51.0	43.6	40.0
Nd	12.6	10.7*	11.5*	15.6	27.5*	12.3*	15.0*	25.1*	19.6	27.1*	21.5*	28.4*	22.1*	24.6*	18.5*
Sm	3.59	2.67*	3.45*	4.22	6.71*	2.25*	2.73*	5.59*	4.90	5.91*	5.24*	5.82*	4.68*	6.63*	4.12*
Eu	1.08	0.91	1.00	1.20	1.67	0.56	0.71	1.46	1.38	1.65	1.47	1.59	1.30	1.49	1.14
Gd	3.49	2.43	3.34	3.40	6.34	1.87	1.95	3.69	4.73	4.88	4.66	4.33	4.67	4.33	3.12
Tb	0.52	0.38	0.56	0.58	0.99	—	—	—	0.64	—	0.75	—	—	0.75	—
Dy	—	—	—	—	—	2.11	2.21	2.47	—	3.95	—	3.31	3.31	—	—
Ho	0.62	0.53	0.62	0.86	1.05	0.41	—	0.45	0.97	0.72	1.06	—	0.66	1.08	—
Er	—	—	—	—	—	1.14	1.48	1.20	—	1.71	—	1.54	1.69	—	1.96
Yb	1.25	1.39	1.35	2.12	2.91	1.02	1.71	1.01	2.09	1.64	2.49	1.38	1.40	2.56	1.75
Lu	0.20	0.22	0.19	0.33	0.41	0.14	0.29	0.18	0.32	0.25	0.39	0.23	0.27	0.37	0.26
Sc	26.0	—	26.1	26.0	19.4	4.8	—	19.6	22.0	—	21.8	—	—	18.6	—
Co	39	29.7	38.3	20.5	29.0	44.3	—	25.2	39.1	—	52.7	—	—	41.0	—
Cr	201	27	205	17	12	5	—	138	147	—	38	—	—	4	—
Cs	1.38	0.95	6.20	1.31	0.44	1.10	—	0.36	0.42	—	0.54	—	—	1.09	—
Hf	1.96	1.55	1.57	2.73	4.70	3.60	—	4.41	3.37	—	4.56	—	—	4.86	—
Ta	0.16	—	0.24	0.27	0.56	0.64	—	0.66	0.65	—	0.75	—	—	0.69	—
Th	1.24	0.88	0.90	1.48	2.69	3.81	—	2.02	1.15	—	2.49	—	—	3.26	—
U	0.55	0.58	0.51	0.72	1.12	1.66	—	0.94	0.45	—	1.15	—	—	1.42	—
$(La/Yb)_n$	5.0	4.0	5.2	3.4	5.0	10.3	6.9	19.0	5.2	12.8	5.7	16.9	11.1	5.4	6.8
Eu/Eu*	0.93	1.02	0.94	0.98	0.79	0.84	0.91	0.99	0.91	0.97	0.93	0.94	0.90	0.93	0.97
Cs/Rb	0.086	0.158	0.230	0.034	0.027	0.023	—	0.021	0.042	—	0.022	—	—	0.027	—
Nb/La	0.63	0.47	0.65	0.43	0.45	0.50	0.39	0.48	0.79	0.34	0.54	0.34	0.64	0.57	0.33

Sample affiliation: P, Pimainus Formation; S, Spius Formation
Method: INAA, instrumental neutron activation analysis; PIGS, pre-irradiation group concentration method
*By mass spectrometry isotope dilution
†By INAA and PIGS

tholeiite field, while samples farther south around Kingsvale follow a calc-alkaline trend. The range of TiO_2 (0.94 to 1.46 wt%) and P_2O_5 (0.20 to 0.51 wt%) contents is large, due to the presence of Spius-like compositions (e.g. samples 101C and 102D) within the mapped extent of the Pimainus Formation, although in most Pimainus samples TiO_2 and P_2O_5 contents are similar to typical arc compositions (Figures 3 and 4). Likewise, trace element ratios such as Nb/La (0.43 to 0.65), and $(Sr/P)_N$ (0.84 to 4.1) are comparable to those of typical arc sequences, although the ranges are extended to low values by the Spius-like compositions. Basaltic to andesitic compositions are LREE-enriched with $(La/Yb)_n$ ratios of 3.4 to 5.2, with flat to sloping HREE patterns similar to medium K arc suites (Figure 5). Eu anomalies ($Eu/Eu^* = 0.93$ to 1.02) are slightly negative or absent. MORB-normalized trace element profiles show enrichment in large ion lithophile elements (LILE), and display the characteristic negative Nb anomaly of arc rocks (Figure 6). Nd–Sr isotopic compositions ($\varepsilon_{Nd}(100Ma) = +5.2$ to $+7.0$, $\varepsilon_{Sr}(100Ma) = -10$ to -20) lie on the mantle array between the ranges for oceanic arcs such as the Mariana arc and continental arcs built on accreted terranes such as the Cascade arc (Figure 7). Measured Pb isotopic compositions ($^{206}Pb/^{204}Pb = 18.82$ to 18.86, $^{207}Pb/^{204}Pb = 15.55$ to 15.59, $^{208}Pb/^{204}Pb = 38.24$ to 38.42) likewise follow a typical arc trend between MORB and sediment compositions, similar to the Cascade arc (Figure 8). Pb abundances were not measured, but as arc volcanics generally have μ values around 9 to 10 (e.g. basalts from the Lassen region, Cascade arc, have $\mu = 9$ to 10; Borg *et al.* 1997), the position of the samples relative to crust/mantle reservoirs on age correction is not likely to change significantly.

Dacite and rhyolite compositions have low Ti contents (less than 0.45 wt%) suggesting the operation of magnetite fractionation (Figure 3). However, their REE patterns and Sr/Y–Y systematics (Figures 5 and 9) indicate

Table 3. Isotope data for Spences Bridge Group volcanic rocks

Sample	$^{87}Rb/^{86}Sr$	$^{87}Sr/^{86}Sr_{meas}$	$^{87}Sr/^{86}Sr_{corr}$	ε_{Sr}	Sm (ppm)	Nd (ppm)	$^{147}Sm/^{144}Nd$	$^{143}Nd/^{144}Nd_{meas}$	$^{143}Nd/^{143}Nd_{corr}$	ε_{Nd}	$^{206}Pb/^{204}Pb$	$^{207}Pb/^{204}Pb$	$^{208}Pb/^{204}Pb$
Pimainus Formation													
101I	0.028	0.70343 ± 2	0.70339	−17.9	2.67	10.7	0.1503	0.512895 ± 16	0.512797	+5.6			
101E	0.089	0.70360 ± 3	0.70347	−16.8	3.45	11.5	0.1806	0.512925 ± 21	0.512807	+5.8			
102C	0.214	0.70383 ± 4	0.70353	−15.9	5.01	20.9	0.1449	0.512963 ± 05	0.512868	+7.0			
370B	0.022	0.70334 ± 2	0.70331	−19.1	4.30	17.2	0.1514	0.512962 ± 07	0.512863	+6.9	18.826	15.555	38.239
101C	0.153	0.70357 ± 2	0.70335	−18.5	6.02	26.5	0.1374	0.512863 ± 26	0.512773	+5.2			
104B	0.086	0.70341 ± 3	0.70329	−19.3	4.23	18.0	0.1428	0.512955 ± 18	0.512862	+6.9			
102D	0.112	0.70342 ± 3	0.70326	−19.8	6.71	29.5	0.1379	0.512912 ± 21	0.512822	+6.1			
106	0.117	0.70371 ± 2	0.70354	−15.8	3.10	17.7	0.1059	0.512847 ± 16	0.512778	+5.2	18.864	15.585	38.426
74B	0.195	0.70361 ± 1	0.70333	−18.7	4.08	18.1	0.1367	0.512956 ± 15	0.512867	+7.0			
102G	0.384	0.70404 ± 2	0.70349	−16.4	2.61	13.9	0.1136	0.512875 ± 08	0.512801	+5.9			
102E	0.374	0.70413 ± 2	0.70360	−14.9	5.13	21.3	0.1455	0.512957 ± 11	0.512862	+6.9			
102F	0.363	0.70403 ± 3	0.70351	−16.2	2.25	12.3	0.1101	0.512871 ± 15	0.512799	+5.7	18.853	15.577	38.373
298C	0.672	0.70443 ± 2	0.70347	−16.8	2.73	15.0	0.1102	0.512892 ± 08	0.512820	+6.1	18.903	15.591	38.427
105	1.156	0.70556 ± 2	0.70392	−10.4									
Spius Formation													
134B	0.067	0.70321 ± 2	0.70311	−21.9	5.59	25.1	0.2079	0.512943+05	0.512807	+5.8	18.857	15.594	38.370
69C	0.135	0.70353 ± 2	0.70334	−18.6	6.49	28.9	0.1358	0.512924 ± 06	0.512835	+6.4			
107	0.080	0.70373 ± 2	0.70362	−14.7	3.96	17.6	0.1361	0.512878 ± 17	0.512789	+5.5	18.830	15.570	38.337
284C	0.025	0.70328 ± 2	0.70324	−20.0	5.91	27.1	0.2448	0.512942 ± 09	0.512782	+5.3			
71D	0.102	0.70330 ± 4	0.70315	−21.3	5.24	21.5	0.1472	0.512935 ± 14	0.512839	+6.4	18.812	15.562	38.271
97B	0.148	0.70315 ± 2	0.70294	−24.3	5.82	28.4	0.1238	0.512921 ± 15	0.512840	+6.5			
292C	0.034	0.70352 ± 3	0.70347	−16.8	4.68	22.1	0.1193	0.512885 ± 08	0.512807	+5.8	18.905	15.567	38.284
149A	0.073	0.70352 ± 3	0.70342	−17.5	4.12	18.5	0.1365	0.512951 ± 21	0.512862	+6.9	18.890	15.581	38.369
70	0.216	0.70358 ± 3	0.70327	−19.6	6.63	24.6	0.1633	0.512908 ± 11	0.512801	+5.7	18.881	15.581	38.378
71A	0.415	0.70394 ± 2	0.70335	−18.5	5.90	28.5	0.1253	0.512927 ± 05	0.512845	+6.6			

Subscripts: meas = measured ratios; corr = ratios corrected to an age of 100 Ma.
ε_{Sr} and ε_{Nd} calculated at 100 Ma
Sm and Nd by mass spectrometry isotope dilution

they are not simple fractionation products of mafic–intermediate compositions. Two groups may be recognized from their FeO*/MgO ratios. Samples 102E, 298C and 105 show iron enrichment with FeO*/MgO = 4.6 to 7.7, have low to medium K contents, Y contents greater than 18 ppm, and Sr/Y ratios similar to typical arc sequences (Figures 2 and 9). Rhyolite 298C has slightly greater LREE enrichment ($La/Yb_n = 6.9$) than the mafic–intermediate samples, but is depleted in the middle REE resulting in a convex curvature to the REE profile (Figure 5). Isotopic compositions of the high FeO*/MgO dacites–rhyolites fall within the range of the less evolved Pimainus samples (Figure 7). Felsic lavas with similar Sr/Y ratios and REE patterns from the Cascade arc have been interpreted as melts of basaltic compositions within the lower continental crust (Borg and Clynne 1998). The isotopic composition of the Pimainus samples would allow derivation from earlier Pimainus arc tholeiite compositions in a comparable model. However, isotopic overlap with low K to shoshonitic lavas of the Triassic Nicola Group ($\varepsilon_{Nd}(220Ma) = +4.9$ to $+7.8$, $\varepsilon_{Sr}(220Ma) = -3$ to -19; Smith *et al.* 1995) which make up the principal volcanic assemblage on the Quesnel terrane (Figure 7), would also allow derivation of felsic Pimainus compositions by melting of accreted terrane material. Interaction of Pimainus mafic to intermediate melts with similar crustal material would explain the lack of isotopic variation with silica content (Figure 4) despite the range of potential crustal contaminant compositions ($\varepsilon_{Nd} = -1.0$ to $+7.5$, $\varepsilon_{Sr} = -20$ to $+90$; Samson *et al.* 1989; Smith *et al.* 1995; Patchett and Gehrels 1997) indicated from terrane sediments.

A second dacite–rhyolite suite is represented by samples 102F and 102G, which have low FeO*/MgO ratios (1.1 to 1.4), and medium to high K_2O contents (Figure 2). Rhyolite 102F shows the greatest LREE enrichment of the Pimainus samples and is also HREE-depleted, resulting in a high La/Yb_n ratio of 10.3. Similarly, Y contents

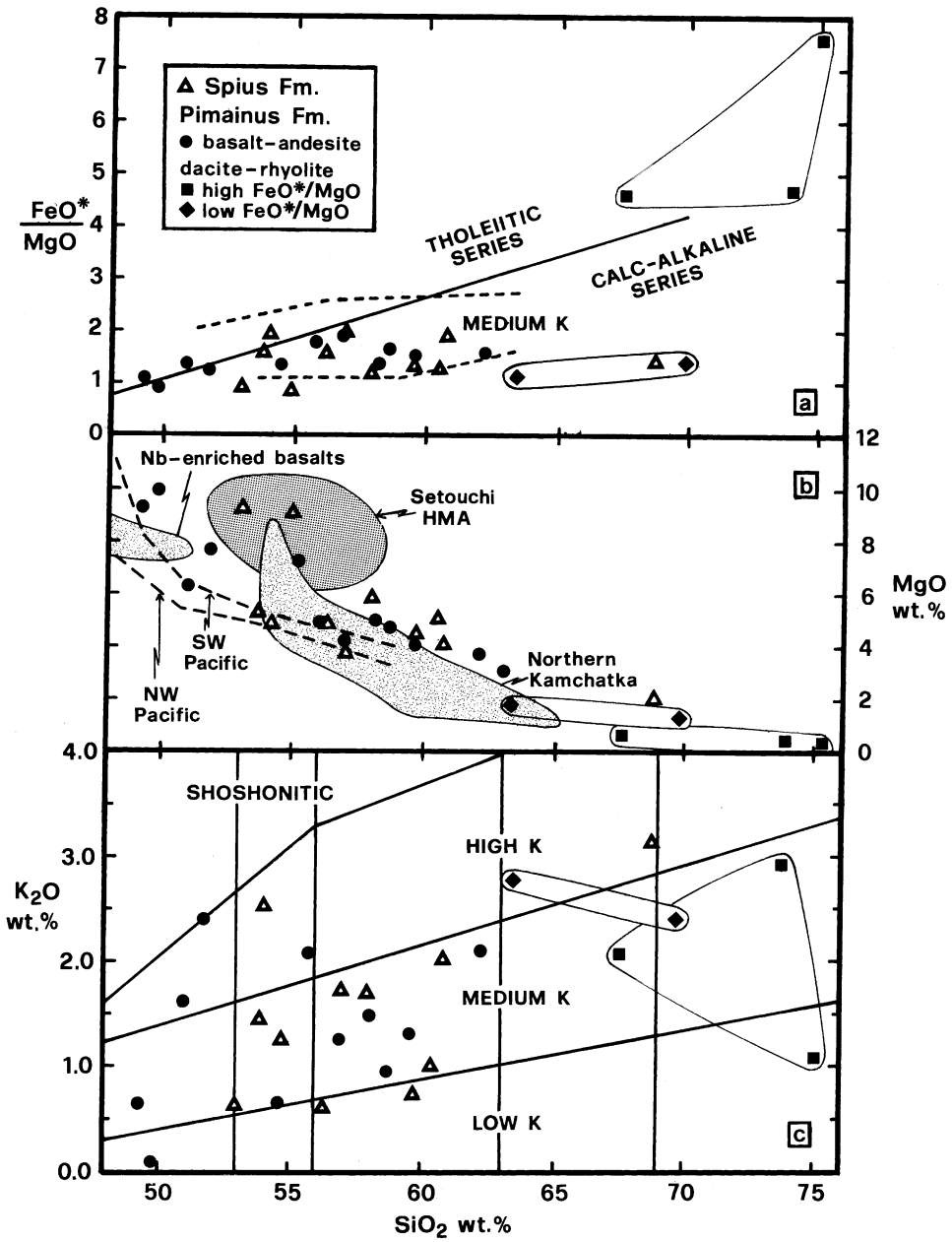

Figure 2. Major element variation in the SBG: (a) FeO*/MgO versus silica. The dividing line between tholeiitic and calc-alkaline compositions is from Miyashiro (1974), with the range (dashed lines) for typical medium-K arc suites from Gill (1981). (b) MgO versus silica. Average trends for arc suites from the northwest and southwest Pacific (dashed lines) are from Ewart (1982). Also shown are fields for Setouchi belt high-Mg andesites (Shimoda *et al.* 1998) and volcanic rocks from the northern Kamchatka arc (Kepezhinskas *et al.* 1997) as an example of compositions in the adakitic association. (c) K_2O versus silica. The division into low-, medium- and high-K and shoshonitic suites is from Tatsumi and Eggins (1995), with vertical lines indicating, from left to right, the division into basalt, basaltic andesite, andesite, dacite and rhyolite compositions.

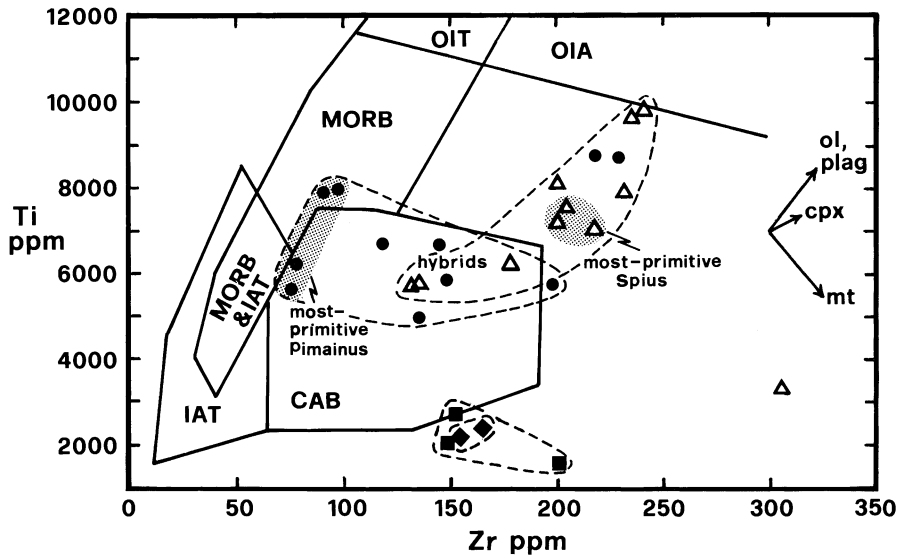

Figure 3. Variations in Ti and Zr content in SBG volcanic rocks. Fields for island arc tholeiites (IAT), MORB, calc-alkaline basalts (CAB), ocean island tholeiites (OIT) and ocean island alkali basalts (OIA) are from Pearce and Cann (1973) and Floyd and Winchester (1975); fractionation vectors are from Pearce and Norry (1979). Dashed lines outline the principal compositional types in the SBG. Symbols are as for Figure 2.

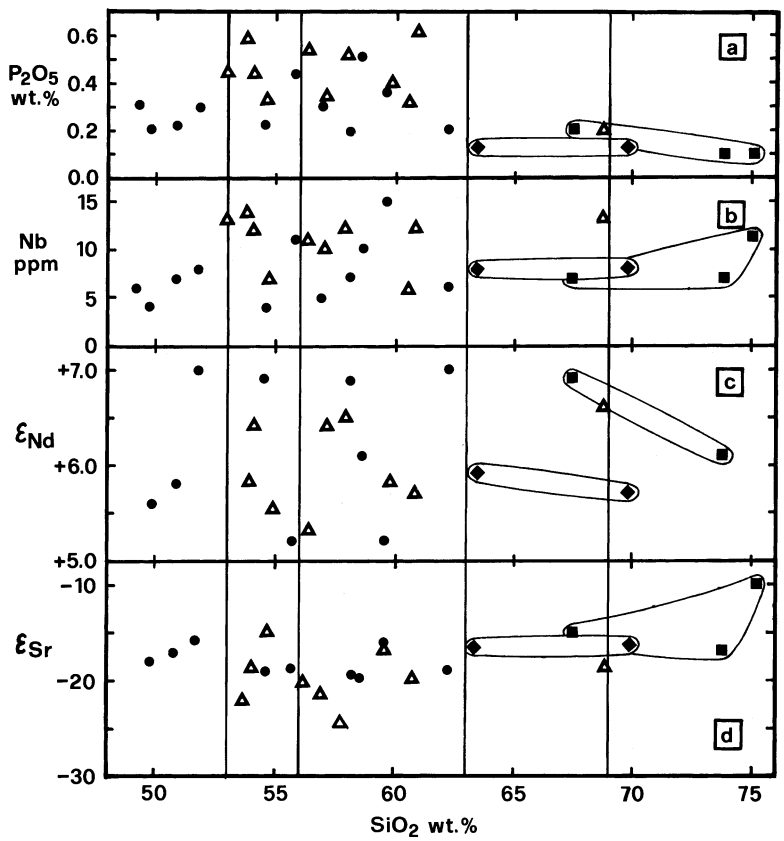

Figure 4. Variation of (a) P_2O_5, (b) Nb, (c) ε_{Nd}, (d) ε_{Sr} with silica content in the SBG. Symbols and division of silica range are as for Figure 2.

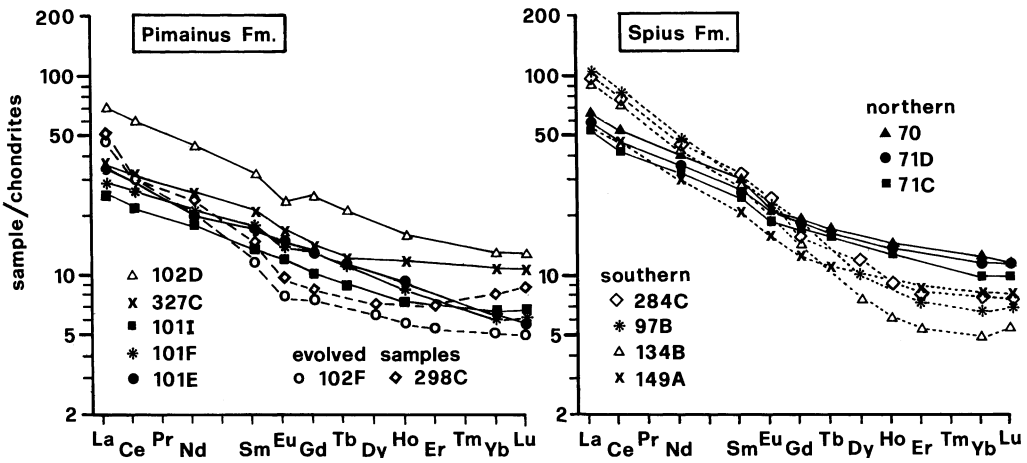

Figure 5. Chondrite-normalized rare earth element patterns of SBG volcanic rocks. Normalizing abundances are from Taylor and Gorton (1977).

(less than 18 ppm) are low, and the samples lie within the adakite field on a graph of Sr/Y-Y (Figure 9), suggesting an origin related to slab melting rather than crustal melting. Other features of adakitic melts shown by these samples include more than 15 wt% Al_2O_3, less than 10 ppm Sc, and Zr/Sm ratios greater than 50, such that their compositions have similarities with dacites from Mount St Helens in the Cascade arc described by Defant and Drummond (1993). However, the Pimainus samples differ from the Cascade dacites in the absence of positive Eu anomalies, and neither do they have the Sr enrichment typical of adakitic suites, although their Sr/P_N ratios of 3.2 to 3.5 are higher than those of samples in the high FeO*/MgO suite ($Sr/P_N = 0.6$ to 2.9). Nd, Sr and Pb isotopic compositions of samples 102G and 102F lie within the range for other Pimainus samples, but differ from the high FeO*/MgO felsic suite in having ε_{Nd} values of less than $+6.0$, whereas the latter have ε_{Nd} values greater than $+6.0$ (Figure 4). Isotopic overlap is observed with Mount St Helens dacites in ε_{Nd}, although Sr isotopic compositions are less radiogenic in the Pimainus samples (Figure 7).

4.2 Spius Formation

The Spius lavas are mostly basaltic andesites and andesites with silica contents from 53 to 61 wt%, although rare dacitic compositions (e.g. sample 71A) are also present. The samples have comparable K_2O contents (0.6 to 2.0 wt%) to intermediate Pimainus compositions, but display a greater range in MgO content (3.8 to 9.2 wt%) and FeO*/MgO ratios (FeO*/MgO = 0.88 to 2.03), with the more Mg-rich compositions resembling high-Mg andesites (Figure 2). Ni and Cr contents (up to 102 and 150 ppm, respectively) are also higher than in the Pimainus samples. Spius lavas also have higher Nb (10 to 14 ppm), Zr (130 to 305 ppm), TiO_2 (0.97 to 1.64 wt%), P_2O_5 (0.34 to 0.61 wt%), and lower $(Sr/P)_N$ (0.9 to 2.6) than their Pimainus counterparts (Figures 4 and 6). In Ti–Zr variation, basaltic andesite and andesite compositions define a V-shaped array between the fields for intraplate and calc-alkaline basalts, with the most primitive samples in terms of Ni and Cr content (samples 97B, 134B, 71C) lying at the apex of the array (Figure 3). The presence of hybrid and Pimainus-like compositions (e.g. samples 107 and 149A) is indicated by the extension of the Ti–Zr into the calc-alkaline basalt field. The steeper segment of the Ti–Zr array follows the olivine–plagioclase fractionation vector, with compositional control by fractionation of olivine supported by a decrease in MgO and Ni with increasing Ti and Zr. Differences between the formations are also seen in LILE, with Spius lavas generally having K/Rb ratios greater than 500 while Pimainus lavas mostly have K/Rb ratios of less than 500. Similarly, Cs/Rb ratios are lower and more mantle-like in the Spius lavas.

The Spius samples also show greater LREE enrichment and HREE depletion than their Pimainus counterparts, although as for the Pimainus, regional variation is apparent as samples from the north of the Spius outcrop area

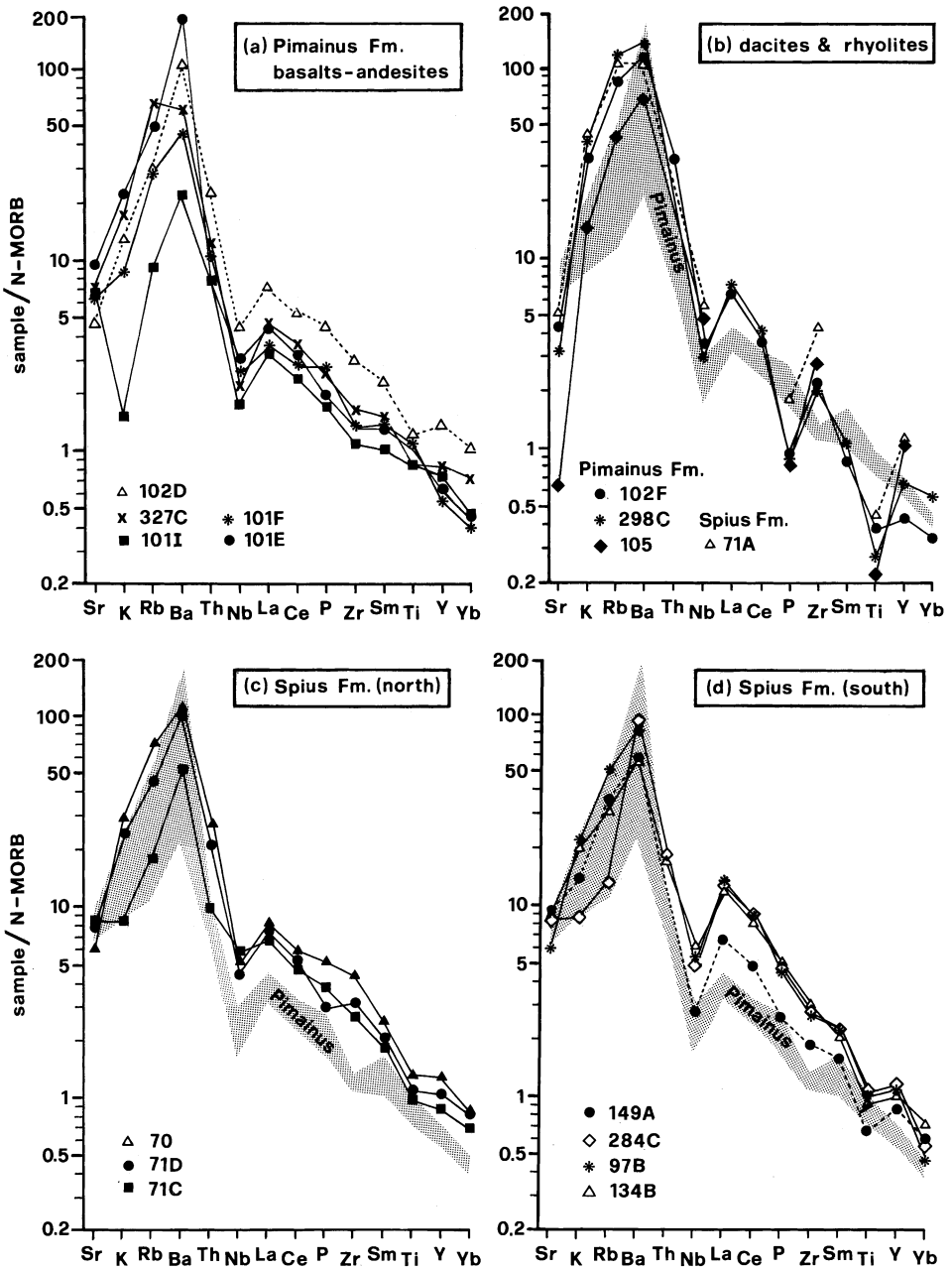

Figure 6. N-MORB normalized trace element profiles for SBG volcanic rocks. Normalizing abundances are from Sun and McDonough (1989). The range for Pimainus basalt–andesite compositions is shaded in (b) to (d) as a reference.

have $(La/Yb)_n = 5$ to 6 and flat HREE with abundances $10\times$ chondritic, whereas Spius samples from the south near Kingsvale have $(La/Yb)_n = 11$ to 19 and concave HREE patterns with abundances as low as $5\times$ chondritic (Figure 5). Eu anomalies are absent or slightly negative as in the Pimainus samples. Spius lavas have less well-developed Nb anomalies in trace element profile (Figure 6), but ratios such as Nb/La (0.33 to 0.79) are comparable to those in the Pimainus samples and indicate a correlation between LREE and HFSE. Spius Nd-Sr isotopic

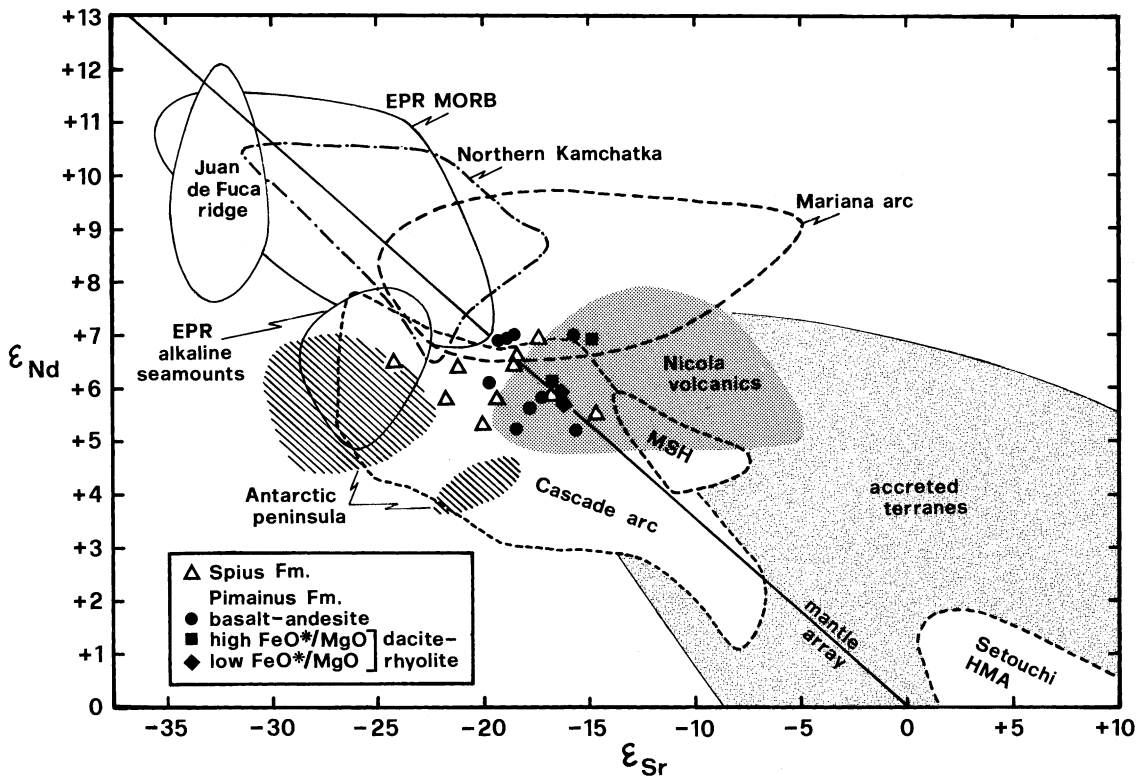

Figure 7. Nd–Sr isotopic variation in SBG volcanic rocks (data corrected to an age of 100 Ma) relative to MORB and seamount basalts from the Juan de Fuca Ridge and East Pacific Rise (EPR) (Zindler *et al.* 1984; Graham *et al.* 1988), arc assemblages related to slab dehydration (Cascade arc: Leeman *et al.* 1990; Borg *et al.* 1997. Mariana arc: DePaolo and Wasserburg 1977; White and Patchett 1984), adakitic assemblages (Setouchi high-Mg andesites: Shimoda *et al.* 1998. Northern Kamchatka arc: Kepezhinskas *et al.* 1997), and basalts erupted in slab window environments (Antarctic peninsula: Hole *et al.* 1995). The range of isotopic compositions of Mount St Helens dacites (MSH) (Halliday *et al.* 1983) with adakite-like high Sr/Y and low Y abundances is also shown, although these samples were not specifically identified as products of slab melting by the authors in their study. Crustal compositions are represented by accreted terrane sediments (Samson *et al.* 1985; Patchett and Gehrels 1997) and volcanic rocks of the Nicola Group (Smith *et al.* 1995).

compositions ($\varepsilon_{Nd}(100Ma) = +5.3$ to $+6.9$, $\varepsilon_{Sr}(100Ma) = -14$ to -25) show some overlap with Pimainus samples at high ε_{Sr} values. However, the low ε_{Sr} values overlap the range for East Pacific Rise alkaline seamount basalts, such that the Spius samples define a trend lying at an angle to the mantle array, somewhat comparable to that shown by volcanic rocks from the Cascade arc (Figure 7). The range of measured Pb isotopic compositions for the Spius samples is similar to that of the Pimainus (Figure 8). The low ε_{Sr} values and enrichments in HFSE give the Spius lavas a mild intraplate character, although Spius compositions are more evolved and arc-like than the basaltic compositions which display HFSE enrichment in other arcs. Nonetheless, the occurrence of the lowest ε_{Sr} values in the samples (97B and 134B) with highest Ni and Cr contents suggests the existence of a distinct Spius magma type.

5. DISCUSSION

Models for the SBG must explain: (1) the presence of adakitic signatures in the Pimainus Formation compared to mild intraplate signatures in the Spius Formation; (2) the transition between Pimainus and Spius types whereby Spius-like compositions are found in the Pimainus Formation and reciprocally, Pimainus-like compositions in the

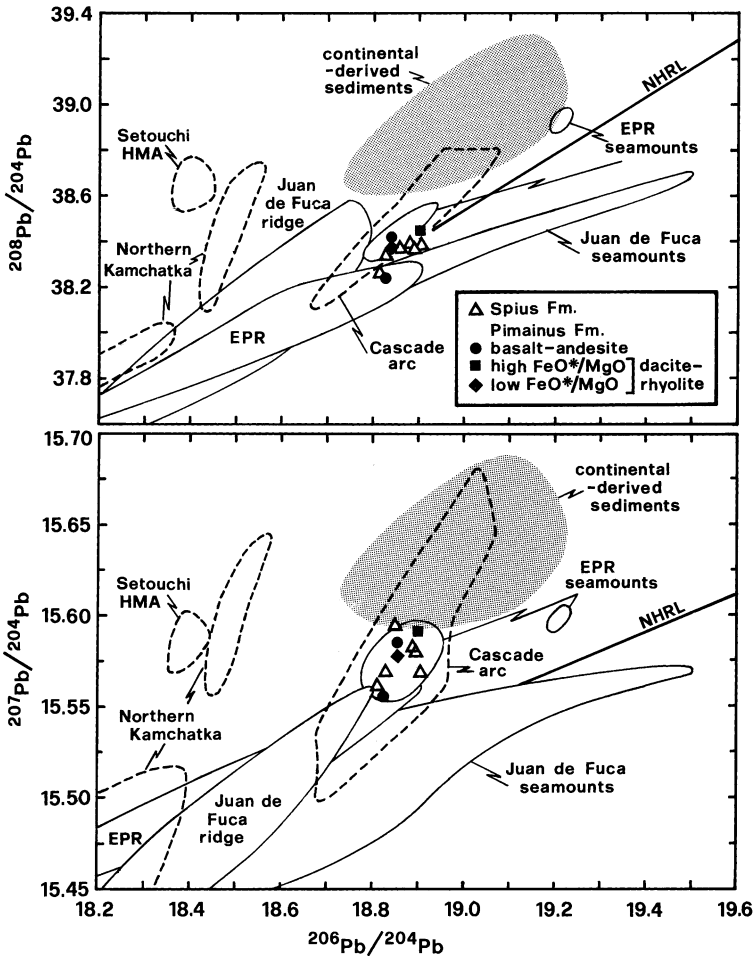

Figure 8. Measured Pb–Pb isotopic compositions of Spences Bridge volcanic rocks. Data sources are as for Figure 7; additionally, Juan de Fuca ridge (Church and Tatsumoto 1975) and continental-derived sediments from the northeast Pacific basin (Church 1976). NHRL is the Northern Hemisphere Reference Line of Hart (1984).

Spius; (3) the range of compositional variation as the low grade of metamorphism suggests it is not the result of alteration; and (4) the regional variation within the arc whereby Pimainus compositions are more tholeiitic in the north and predominantly calc-alkaline in the south of the study area. In consideration of the wide range of models that have been proposed for arc volcanism, the roles of metasomatism and source region heterogeneity are first examined with reference to a Nd-Sr isotopic mixing model in order to identify the nature of the source components involved before considering possible tectonic settings in which such components could be found.

5.1 Slab dehydration and lithospheric heterogeneity

In modern subduction zones, slab dehydration is generally thought to predominate over slab melting (e.g. Gill 1981; Tatsumi and Eggins 1995). As the slab dehydrates, LILE and LREE are partitioned into the fluid phase which then reacts with the hanging wall mantle to form amphibole-bearing peridotites. Corner flow in the mantle wedge then downdrags the hanging-wall assemblages which subsequently begin to melt as the amphibole solidus is exceeded. Alkali elements are fractionated in slab fluids (Tatsumi *et al.* 1986), such that high Cs/Rb (and correspondingly low K/Rb) ratios in mafic tholeiitic compositions of the Pimainus Formation where Cs/Rb ranges from

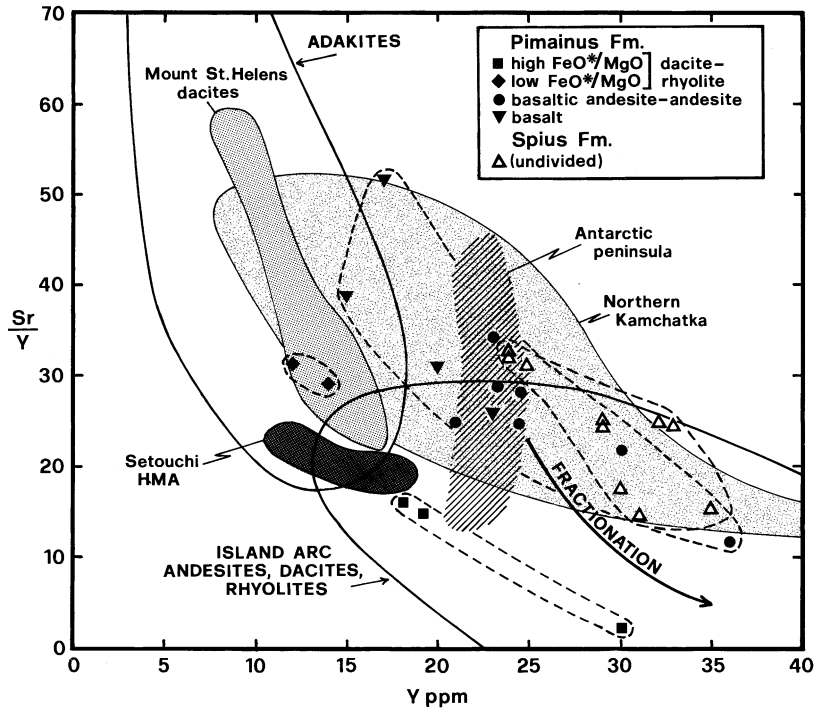

Figure 9. Sr–Y variation in the SBG and other volcanic suites (Antarctic peninsula slab window basalts: Hole *et al.* 1995. Mount St Helens dacites: Defant and Drummond 1993. Northern Kamchatka arc volcanics: Kepezhinskas *et al.* 1997. Setouchi high-Mg andesites: Shimoda *et al.* 1998) on the discrimination diagram of Defant and Drummond (1993) for recognition of intermediate to felsic arc suites related to slab dehydration and slab melting. Dashed lines illustrate the principal compositional suites in the SBG. Bold arrow indicates the fractionation path calculated by Defant and Drummond (1993) for melts crystallizing an assemblage of clinopyroxene, orthopyroxene and plagioclase.

0.08 to 0.23, are consistent with this type of metasomatism. The isotopic composition of the slab-derived fluid depends on the contributions from the basalt and sediment portions of the slab (curve 1, Figure 10a). The mixing curve between mantle wedge and fluid compositions is convex because of the high Sr/Nd ratio expected in the fluid phase (curve 2, Figure 10a). However, if the volume of fluid is large, the metasomatized composition lies close to that of the basalt–sediment mixing line. Using average MORB and terrane sediment compositions, a fluid–metasomatized mantle wedge composition can be calculated which lies within, or to the right of the high ε_{Sr}, high ε_{Nd} compositions seen in the Pimainus Formation. Alternative sediment compositions, such as the Gorda ridge sediment ($\varepsilon_{Nd} = -5.8$, $\varepsilon_{Sr} = +70$) used by Borg *et al.* (1997) in modelling the Cascade arc, would not produce any significant changes to the shape of the mixing curves. It is therefore difficult to explain the low ε_{Nd}–low ε_{Sr} compositions of Pimainus samples which lie below the mantle array, by fluid metasomatism alone. Similarly, the fluid metasomatism model fails to explain the isotopic compositions of the Spius samples, which as for HFSE-enriched compositions in other arcs, must be explained by a reduction of metasomatic input and tapping of pre-existing source components.

As noted by Leeman *et al.* (1990), mantle beneath accreted terranes is likely to comprise slivers of oceanic mantle formerly associated with the overlying crustal assemblages, and might therefore include residual source assemblages, or have been veined by melts similar to those found in the crustal assemblages during the previous episodes of volcanism. The isotopic overlap of Pimainus compositions with Nicola Group volcanic rocks of the Quesnel terrane, noted in section 4.1, indicates that remnants of the earlier Nicola source regions in the mantle wedge could be a potential contaminant for SBG lavas in the southern part of the study area. In contrast, lithospheric mantle beneath the SBG exposures in the northern part of the study area may have formerly been associated with the

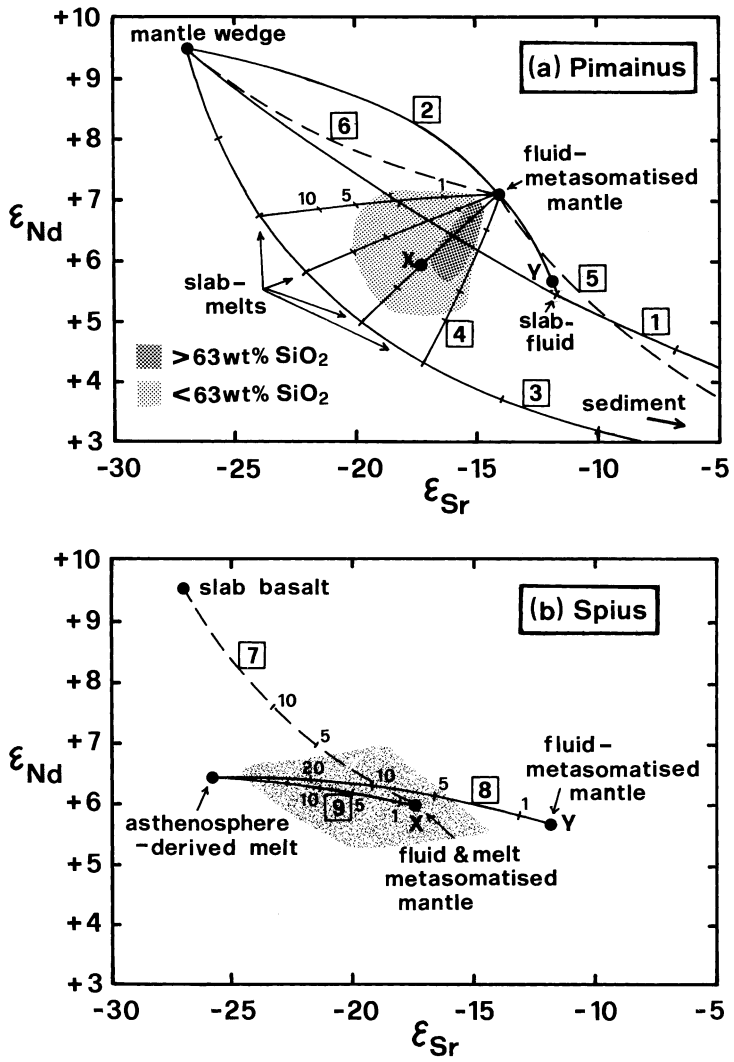

Figure 10. Mixing models for generation of Nd–Sr isotopic compositions in (a) Pimainus Formation (b) Spius Formation samples. Numbers in square boxes indicate the sequence of mixing line calculations: 1, calculation of slab fluid composition from slab basalt and slab sediment compositions; 2, fluid (derived from 80:20 basalt:sediment mix as illustrated) metasomatism of the mantle wedge; 3, calculation of slab melt compositions where, for simplicity, it is assumed that the sediment component undergoes complete melting; 4,5,6, metasomatism of a mantle wedge previously metasomatized with slab fluids by a slab melt derived from basalt–sediment mixtures, slab sediment, and slab basalt, respectively; 7, infiltration of melts derived from slab basalt into a mantle wedge which had previously undergone metasomatism by fluids and melts derived from slab basalt-sediment mixtures; 8, metasomatism of a fluid-metasomatized mantle wedge by small melt fractions derived from the asthenosphere; 9, metasomatism of a fluid and melt-metasomatized mantle wedge by small melt fractions derived from the asthenosphere. Points X and Y are for reference and represent fluid- and melt- and fluid-metasomatized mantle wedge compositions, respectively. Tick marks on mixing curves indicate 10% increments unless otherwise indicated. Components: slab basalt: 7.3 ppm Nd, 90 ppm Sr (Sun and McDonough 1989), $\varepsilon_{Nd} = +9.5$, $\varepsilon_{Sr} = -27$ (median of East Pacific Rise basalt compositions); slab sediment: 34.5 ppm Nd, 254 ppm Sr (Pacific sediment of Borg *et al.* 1997), $\varepsilon_{Nd} = +2.0$, $\varepsilon_{Sr} = +10$ (average accreted terrane sediment); mantle wedge peridotite: 0.654 ppm Nd, 5.77 ppm Sr (MORB-source of Borg *et al.* 1997), $\varepsilon_{Nd} = +9.5$, $\varepsilon_{Sr} = -27$ (assumed to be the same as slab basalt); adakite melt: 15 ppm Nd, 706 ppm Sr (average adakite of Martin 1999), $\varepsilon_{Nd} = +9.5$, $\varepsilon_{Sr} = -27$ (assumed to be the same as slab basalt); sediment melt 34.5 ppm Nd, 254 ppm Sr, $\varepsilon_{Nd} = +2.0$, $\varepsilon_{Sr} = +10$ (as for slab sediment assuming 100% melting); asthenospheric small melt fraction: 31.5 ppm Nd, 420 ppm Sr, $\varepsilon_{Nd} = +6.4$, $\varepsilon_{Sr} = -25.7$ (average of four alkaline seamount basalts from Graham *et al.* 1988).

Cache Creek terrane, which includes ocean island basalt types and would therefore be suitable for imparting elevated HFSE abundances. However, basalts in the Cache Creek terrane show a wide range of Pb compositions (Smith and Lambert 1995), and therefore would be unsuitable as a contaminant in consideration of the limited range of Pb isotopic variation seen in the Spius Formation. Mild intraplate signatures have also been ascribed to generation of melts from sediments in the mantle wedge (Leeman *et al.* 1990; Borg *et al.* 1997). However, as sediments have higher Cs/Rb than mantle compositions, the ratios in the SBG are the reverse of what would be expected if the HFSE abundances in the Spius Formation were derived from sediment, notwithstanding that the low $^{87}Sr/^{86}Sr$ ratios in the Spius Formation would also be unrealistic for a sediment source. Models involving slab dehydration or lithospheric heterogeneity cannot therefore explain the progression from Pimainus to Spius compositions.

5.2 Slab melting processes

The presence of adakitic signatures in dacite and rhyolite compositions in the Pimainus Formation requires evaluation of the role of slab melts in the generation of the SBG. As noted by Defant and Kepezhinskas (2001), strongly developed adakitic signatures are not likely to be observed until there has been extensive melt infiltration into the mantle wedge. Generation of calc-alkaline melts as the result of melt metasomatism (e.g. Bau and Knittel 1993) may represent the earliest stage of adakitic metasomatism, while production of high Mg-andesites as silicic melts react with the mantle wedge peridotite (Kay 1978; Kelemen 1995; Martin 1999) may constitute an intermediate stage. Melt metasomatism could therefore account for the high MgO contents of Pimainus andesites, and the potential would also exist for a range of K_2O and HFSE contents to be imparted from interaction of melts with amphibole stabilized in the mantle wedge during any earlier stage of fluid metasomatism. Models for the generation of adakite suites have generally invoked melting of the basaltic part of the slab as most adakites have MORB-like isotopic compositions (e.g. Yogodzinski *et al.* 1994; Kepezhinskas *et al.* 1997; Sajona *et al.* 2000). However, high-Mg andesites in the Setouchi belt of southwest Japan display high ε_{Sr} and low ε_{Nd} (Figure 7) and have been interpreted as melts of the sediment layer of the subducting slab (Shimoda *et al.* 1998). The Setouchi andesites lack positive Eu anomalies and have low Sr abundances, similar to the felsic Pimainus compositions with low FeO*/MgO, the features having been interpreted to result from residual plagioclase during the melting of sediment (Shimoda *et al.* 1998). However, the limited isotopic overlap of Pimainus dacite–rhyolite compositions with terrane sediments renders a pure sediment source unlikely. Rather, as slab melt compositions would lie on a concave Nd-Sr isotopic mixing curve passing to the left of the Pimainus field (curve 3, Figure 10a), Pimainus compositions, including those of the felsic rocks, can be fitted by the addition of up to 10% melt derived from a slab with 20% to 50% sediment component, into a previously fluid-metasomatized mantle wedge (curve 4, Figure 10a).

The question then arises as to whether Spius volcanism might be related to a more advanced stage of melt metasomatism. Spius Nd-Sr isotopic compositions also lie along mixing lines between slab basalt–sediment melts and fluid-metasomatized mantle wedge compositions, particularly if a composition (e.g. Y, Figure 10) with lower ε_{Nd} and ε_{Sr} than invoked in the generation of Pimainus compositions is chosen for the mantle wedge. However, generation of the lowest ε_{Sr} values would require virtually a pure slab melt composition which would be unrealistic as Spius lavas show few features of adakite melts. A more feasible method of generating low ε_{Sr} values would be to invoke metasomatism by an adakitic melt from the basaltic part of the subducting slab, as the high Sr/Nd ratios found in adakites (e.g. Martin 1999) could impart a curvature towards low ε_{Sr} in isotopic mixing calculations. However, as shown in Figure 10 (curves 6 and 7), introduction of an adakite melt with an isotopic composition corresponding to that of average East Pacific Rise MORB into either a fluid- or fluid-melt-metasomatised peridotite only reproduces part of the Sr isotopic range seen in the Spius Formation. Generation of the lowest ε_{Sr} values would be possible with a slab melt having the isotopic composition of Juan de Fuca ridge MORB ($\varepsilon_{Sr} = -32.5$, $\varepsilon_{Nd} = +8.5$), but unradiogenic Sr isotopic compositions are unlikely in consideration of probable hydrothermal alteration of oceanic crust. Melting of a MORB composition would also be expected to produce a sinuous REE pattern, with HREE depletion from residual garnet, and relatively low La/Sm inherited from the original LREE-depleted character of the basalt (Saunders *et al.* 1987). Spius lavas have the requisite HREE depletion, but they are

enriched in LREE, such that an adakite metasomatism model would have to involve small enough degrees of melting to offset the LREE depletion of the source basalt. But even invoking metasomatism by small melt fractions as in models for the origin of Nb-enriched arc basalts (e.g. Defant and Kepezhinskas 2001), it is doubtful if a melt composition would have the necessary Sr/Nd ratio (in excess of 100 using the compositions in Figure 10) to produce the curvature of the mixing lines required to generate the Spius array. Small melt fractions derived from subducted oceanic crust would also be expected to have high Sr/Y ratios (Defant and Drummond 1993), and should therefore produce a trend toward adakitic compositions, whereas Spius compositions lie within the field for arc lavas and asthenospheric melts in Figure 9.

5.3 Asthenospheric sources

Difficulties with the melt metasomatism model for the generation of Spius isotopic composition could perhaps be avoided by invoking melting of a feature such as an alkaline seamount, where basalts have similar isotopic composition to the low ε_{Sr} Spius compositions and are LREE enriched. While such a scenario cannot be precluded, alkaline seamount basalts are comparatively rare on the ocean floor, whereas the source heterogeneities that impart their geochemical signature are a ubiquitous part of the asthenosphere (Zindler *et al.* 1984; Graham *et al.* 1988). Tapping of the low-melting-point amphibole- or pyroxene-bearing components in the asthenosphere which otherwise get diluted in the generation of tholeiitic basalts, provides a more likely source for the low ε_{Sr} component in the SBG. Infiltration of asthenospheric melts having the same composition as alkaline seamount basalts into either a fluid- or fluid-and melt-metasomatized mantle wedge readily reproduces the Spius isotopic array as shown by curves 8 and 9 in Figure 10b. The latter is considered the more viable host as it would be more suitable for generation of the high silica and MgO contents of the Spius samples compared to the basaltic nature of HFSE-enriched types in other arcs. The calculation is relatively insensitive to the amount of previous metasomatism as any decrease in Nd, Sr content in the mantle wedge as the slab metasomatic component decreases, is offset by a shift to higher ε_{Sr}. The mixing lines are most sensitive to the parameters chosen for the asthenospheric melt component, and substituting an average slab window basalt composition of Hole *et al.* (1995) (Figure 7) would alter the proportions of asthenospheric melt to slab melt required to generate the lowest ε_{Sr} of the Spius lavas from 30:70 to 15:85. Asthenospheric melts also have low Cs/Rb and similar Sr/Y to the Spius compositions; hence the model accounts for the trace element features of the Spius lavas, and as seamounts and arcs may have similar Pb isotopic composition, also explains the overlap between Spius and Pimainus lavas in Pb isotopic composition.

5.4 Tectonic scenarios

The evidence for slab melting in the generation of the Pimainus lavas points towards an elevated thermal regime in the subducting slab. In modern arcs, such regimes are mostly related to subduction of young oceanic crust (e.g. Defant and Kepezhinskas 2001), thereby implying the approach of an ocean ridge system toward the continental margin in the mid-Cretaceous. Adakitic dacites and basalts with mild intraplate signatures are found in arcs such as the Cascades where young oceanic crust is being subducted (Leeman *et al.* 1990; Defant and Drummond 1993; Borg *et al.* 1997). However, cross-strike geochemical variation predominates in the Cascade arc, and although adakitic dacites and basaltic compositions with intraplate signatures have been described from Mount St Helens in the fore-arc (Halliday *et al.* 1983; Defant and Drummond 1993), the HFSE-enriched compositions are found mainly toward the back-arc region (Leeman *et al.* 1990; Borg *et al.* 1997). The along-strike distribution of compositional types in the SBG is more like that in the Garibaldi arc which forms the northernmost extension of the Cascade arc. The age of the oceanic crust subducting beneath the Garibaldi arc shows a progressive decrease northwards to where the Explorer ridge intersects the continental margin, and is accompanied by a progression to tholeiitic and alkalic volcanism (Harry and Green 1999). The correlation of increasing intraplate character with decreasing age of the subducting crust was interpreted by Harry and Green (1999) to reflect early dehydration of the slab allowing melting of less-metasomatized components in the mantle wedge. A comparable setting for the SBG might explain the spatial and temporal variations between the Pimainus and Spius Formations as the dehydration front would migrate as progressively younger crust was subducted. However, the model would have

to be combined with the competing concept of slab melting to account for the signatures in the Pimainus Formation, and would therefore encounter difficulties in explaining the proximity of adakitic compositions in the Pimainus Formation to mildly intraplate types in the Spius Formation around Spences Bridge.

Ridge–continent interaction may also lead to ridge subduction and the development of slab window environments (Thorkelson and Taylor 1989; Hole *et al.* 1991; Thorkelson 1996). Volcanism within the slab window results from adiabatic decompression of the asthenosphere as it fills the region where lithosphere was previously subducted, and includes tholeiitic and alkalic basalts, the latter having isotopic signatures similar to alkaline seamount basalts (Hole *et al.* 1995) (Figure 7). Adakitic melts may also be generated along the margins of the slabs bounding the window (Johnston and Thorkelson 1997; Defant and Kepezhinskas 2001), which makes the model attractive to explain the proximity of adakitic and HFSE-enriched types in the SBG. Difficulties with the slab window model are the restricted extent of the Spius Formation relative to the size of slab windows that have been developed in other arcs, and the narrow timespan of SBG eruptions, as alkalic volcanism in slab window environments may post-date development of the window by up to 50 million years (Hole *et al.* 1991, 1995). However, it is possible that strata between Spences Bridge and Kingsvale may be related to only the southern margin of a window developed along a segment of the Spences Bridge arc toward central British Columbia. Volcanism with HFSE-enriched signatures concurrent with arc activity may also be found above the slab, near the margins of the window, as in the example of Turriabla volcano (Reagan and Gill 1989) relative to the Cocos–Nazca slab window proposed by Johnston and Thorkelson (1997).

Asthenospheric upwelling could also have been triggered by roll-back of the subducting slab, as suggested by Hole *et al.* (1995) for the generation of alkalic basalts of the James Ross Volcanic Group in Antarctica. Melting of the asthenosphere in such a scenario takes place by adiabatic upwelling as for the slab window model; however, the length of the melting section is less as mantle flow is largely horizontal with upwelling only into the region of lithospheric extension caused by retreat of the slab (Hole *et al.* 1995). The time period between arc volcanism and invasion of the mantle wedge by asthenospheric melts is therefore reduced. As the former arc source will also be subject to adiabatic melting, the resulting melts would be expected to show features of both high MgO andesites generated from the mantle wedge and alkalic basalts generated from the asthenosphere, as observed in the compositions in the Spius Formation. In the case of the SBG, roll-back may have accompanied termination of ridge spreading as the Methow–Tyaughton basin closed. Slab-hinge roll-back would be expected to have affected much of the length of the volcanic arc; however, the eruption of Spius melts may have been confined by lithospheric thickening on accretion of the Insular terrane to a restricted segment around the suture between the Cache Creek and Quesnel terranes.

6. CONCLUSIONS

The Pimainus Formation of the SBG constitutes an evolved continental arc sequence related to mid-Cretaceous subduction beneath accreted terranes of the North American Cordillera. Lack of evidence for crustal contamination likely reflects compositional similarities between arc magmas and the young crustal section, but while compositions may have been influenced by interaction with the lithosphere, the principal geochemical features of the SBG result from the evolving tectonic conditions which introduced different metasomatic components into the mantle wedge. Arc tholeiites within the Pimainus Formation may be accounted for by slab dehydration models. However, the involvement of slab melts in metasomatism of the mantle wedge is inferred from the high MgO contents of intermediate SBG lavas and the trace element systematics of dacite–rhyolite compositions in the Pimainus Formation. Modelling of Nd-Sr isotopic compositions indicates derivation of the metasomatizing melt from both basaltic and sediment layers of the slab. Subsequent volcanism in the Spius Formation involved a progression to andesitic compositions characterized by low ε_{Sr} and HFSE enrichment, with varying degrees of Pimainus-like features being inherited from both the source of the earlier volcanism and from contamination with Pimainus melts at higher levels in the lithosphere. Slab melting models can only account for the low ε_{Sr} values of the more primitive Spius compositions with difficulty, and the isotopic composition and evolved silica

contents of the Spius Formation are most readily explained by the invasion of small melt fractions from the asthenosphere into a mantle wedge which had already undergone metasomatism by slab melts during generation of the Pimainus Formation. The association of arc tholeiites, calc-alkaline melts, adakitic dacite–rhyolite compositions, and HFSE-enriched andesites in the SBG could have arisen in a range of tectonic scenarios involving the approach of an ocean ridge system to the continental margin during the final stages of closure of the Methow–Tyaughton basin, although the slab-hinge roll-back model offers the best explanation of the geochemical features of the Spius lavas.

ACKNOWLEDGEMENTS

D. Lentz and G. Pe-Piper are thanked for constructive reviews.

REFERENCES

Bau M, Knittel U. 1993. Significance of slab-derived partial melts and aqueous fluids for the genesis of tholeiitic and calc-alkaline island-arc basalts: evidence from Mt. Arayat, Philippines. *Chemical Geology* **105**: 233–251.

Borg LE, Clynne MA. 1998. The petrogenesis of felsic calc-alkaline magmas from the southernmost Cascades, California: origin by partial melting of basaltic lower crust. *Journal of Petrology* **39**: 1197–1222.

Borg LE, Clynne MA, Bullen TD. 1997. The variable role of slab-derived fluids in the generation of a suite of primitive calc-alkaline lavas from the southernmost Cascades, California. *Canadian Mineralogist* **35**: 425–452.

Church SE. 1976. The Cascade Mountains revisited: a re-evaluation in light of new lead isotopic data. *Earth and Planetary Science Letters* **29**: 175–188.

Church SE, Tatsumoto M. 1975. Lead isotopic relations in oceanic ridge basalts from the Juan de Fuca- Gorda ridge area, N.E. Pacific Ocean. *Contributions to Mineralogy and Petrology* **53**: 253–279.

Defant MJ, Drummond MS. 1990. Derivation of some modern arc magmas by melting of young subducted lithosphere. *Nature* **347**: 622–665.

Defant MJ, Drummond MS. 1993. Mount St. Helens: potential example of the partial melting of the subducted lithosphere in a volcanic arc. *Geology* **21**: 547–550.

Defant MJ, Kepezhinskas P. 2001. Evidence suggests slab melting in arc magmas. *Eos* **82**: 65–69.

DePaolo DJ, Wasserburg GJ. 1977. The sources of island arcs as indicated by Nd and Sr isotopic studies. *Geophysical Research Letters* **4**: 465–468.

Duffell S, McTaggart KC. 1952. *Ashcroft map-area, British Columbia.* Memoir 262. Geological Survey of Canada.

Ewart A. 1982. The mineralogy and petrology of Tertiary-Recent orogenic volcanic rocks: with special reference to the andesitic-basaltic compositional range. In *Andesites*, Thorpe RS (ed.). Wiley: Chichester; 25–95.

Floyd PA, Winchester JA. 1975. Magma-type and tectonic setting discrimination using immobile elements. *Earth and Planetary Science Letters* **27** : 211–218.

Gill JB. 1981. *Orogenic Andesites and Plate Tectonics*, Springer-Verlag: Berlin-Heidelberg.

Gill JB, Whelan P. 1989. Postsubduction ocean island alkali basalts in Fiji. *Journal of Geophysical Research* **94**: 4579–4588.

Graham DW, Zindler A, Kurz MD, Jenkins WJ, Batiza R, Staudigel H. 1988. He, Pb, Sr, and Nd isotope constraints on magma genesis and mantle heterogeneity beneath young Pacific seamounts. *Contributions to Mineralogy and. Petrology* **99**: 446–463.

Halliday AN, Fallick AE, Dickin AP, Mackenzie AB, Stephens WE, Hildreth W. 1983. The isotopic and chemical evolution of Mount St.Helens. *Earth and Planetary Science Letters* **63**: 241–256.

Harry DL, Green NL. 1999. Slab dehydration and basalt petrogenesis in subduction systems involving very young oceanic lithosphere. *Chemical Geology* **160**: 309–333.

Hart SR. 1984. A large-scale isotope anomaly in the southern hemisphere mantle. *Nature* **309**: 753–757.

Hole MJ, Rogers G, Saunders AD, Storey M. 1991. Relation between alkalic volcanism and slab-window formation. *Geology* **19**: 657–660.

Hole MJ, Saunders AD, Rogers G, Sykes MA. 1995. The relationship between alkaline magmatism, lithospheric extension and slab window formation along continental destructive plate margins. In *Volcanism Associated with Extension at Consuming Plate Margins*, Smellie JL (ed.). Special Publication 81. Geological Society: London; 265–285.

Irving E, Thorkelson DJ. 1990. On determining paleohorizontal and latitudinal shifts: paleomagnetism of Spences Bridge Group, British Columbia. *Journal of Geophysical Research* **95**: 19213–19234.

Johnston ST, Thorkelson DJ. 1997. Cocos-Nazca slab window beneath Central America. *Earth and Planetary Science Letters* **146**: 465–474.

Journeay JM, Friedman RM. 1993. The Coast Belt thrust system: evidence of Late Cretaceous shortening in southwestern British Columbia. *Tectonics* **12**: 756–775.

Kay RW. 1978. Aleutian magnesian andesites: melts from subducted Pacific Ocean crust. *Journal of Volcanology and Geothermal Research* **4**: 117–132.

Kelemen PB. 1995. Genesis of high Mg# andesites and the continental crust. *Contributions to Mineralogy and Petrology* **120**: 1–19.

Kepezhinskas P, McDermott F, Defant MJ, Hochstaedter A, Drummond MS, Hawkesworth CJ, Koloskov A, Maury RC, Bellon H. 1997. Trace element and Sr-Nd-Pb isotope constraints on a three-component model of Kamchatka arc petrogenesis. *Geochimica Cosmochimica Acta* **61**: 577–600.

Kushiro I. 1975. On the nature of silicate melt and its significance in magma genesis: regularities in the shift of the liquidus boundaries involving olivine, pyroxene and silica minerals. *American Journal of Science* **275**: 411–431.
Leeman WP, Smith DR, Hildreth W, Palacz Z, Rogers N. 1990. Compositional diversity of Late Cenozoic basalts in a transect across the southern Washington Cascades: implications for subduction zone magmatism. *Journal of Geophysical Research* **95**: 19561–19582.
Martin H. 1999. Adakitic magmas: modern analogues of Archean granitoids. *Lithos* **46**: 411–429.
Miyashiro A. 1974. Volcanic rock series in islands arcs and active continental margins. *American Journal of Science* **274**: 321–355.
Monger JWH, Berg HC. 1987. Lithotectonic terrane map of western Canada and southeastern Alaska. In *Lithotectonic Terrane Map of the North American Cordillera*, Silberling NJ, Jones DL (eds). United States Geological Survey, Map 1874B.
Monger JWH, McMillan WJ. 1984. *Bedrock geology of Ashcroft (92I) map area.* Open File Report 980. Geological Survey of Canada.
Patchett PJ, Gehrels GE. 1997. Continental influence on Canadian Cordilleran terranes from Nd isotopic study, and significance for crustal growth processes. *Journal of Geology* **106**: 269–280.
Pearce JA. 1982. Trace element characteristics of lavas from destructive plate boundaries. In *Andesites*, Thorpe RS (ed.). Wiley: Chichester; 525–548.
Pearce JA, Cann JA. 1973. Tectonic setting of basic volcanic rocks determined using trace element analyses. *Earth and Planetary Science Letters* **19**: 290–300.
Pearce JA, Norry MJ. 1979. Petrogenetic implications of Ti, Zr, Y and Nb variations in volcanic rocks. *Contributions to Mineralogy and Petrology* **69**: 33–47.
Ray GE. 1986. The Hozameen fault system and related Coquihalla serpentine belt of southwestern British Columbia. *Canadian Journal of Earth Sciences* **23**: 1022–1041.
Reagan MK, Gill JB. 1989. Co-existing calc-alkaline and high-niobium basalts from Turriabla volcano, Costa Rica: implications for residual titanate in arc magma sources. *Journal of Geophysical Research* **94**: 4619–4633.
Sajona FG, Maury RC, Pubellier M, Leterrier J, Bellon H, Cotton J. 2000. Magmatic source enrichment by slab-derived melts in a young post-collisional setting, central Mindanao (Philippines). *Lithos* **54**: 173–206.
Samson SD, McClelland WC, Patchett PJ, Gehrels GE, Anderson RG. 1989. Evidence from neodymium isotopes for mantle contributions to Phanerozoic crustal genesis in the Canadian Cordillera. *Nature* **337**: 705–709.
Saunders AD, Rogers G, Marriner GF, Terrell DJ, Verma SP. 1987. Geochemistry of Cenozoic volcanic rocks, Baja California, Mexico: Implications for the petrogenesis of post–subduction magmas. *Journal of Volcanology and Geothermal Research* **32**: 223–245.
Shimoda G, Tatsumi Y, Nodha S, Ishizaka K, Jahn BM. 1998. Setouchi high-Mg andesites revisited: geochemical evidence for melting of subducting sediments. *Earth and Planetary Science Letters* **160**: 479–492.
Smith AD. 1993. Geochemistry and tectonic setting of basalts from the Anyox mining camp, British Columbia. *Canadian Journal of Earth Sciences* **30**: 48–59.
Smith AD, Lambert RStJ. 1995. Nd, Sr, and Pb isotopic evidence for contrasting origins of Late Paleozoic volcanic rocks from the Slide Mountain and Cache Creek terranes, south-central British Columbia. *Canadian Journal of Earth Sciences* **32**: 447–459.
Smith AD, Gillis KM, Ludden JN. 1990. A *P*re-*I*rradiation *G*roup *S*eparation (PIGS) technique for the determination of rare earth elements during Nd isotopic analysis of geological samples. *Chemical Geology* **81**: 17–22.
Smith AD, Brandon AD, Lambert RStJ. 1995. Nd-Sr isotope systematics of Nicola Group volcanic rocks, Quesnel terrane. *Canadian Journal of Earth Sciences* **32**: 437–446.
Souther JG. 1991. Volcanic regimes. In *Geology of the Cordilleran Orogen in Canada,* Gabrielse H, Yorath CJ (eds). Geological Survey of Canada: 457–490 (also Geological Society of America, *The Geology of North America*, volume G2).
Sun SS, McDonough WF. 1989. Chemical and isotopic systematics of oceanic basalts: implications for mantle composition and processes. In *Magmatism in the Ocean Basins*, Saunders AD, Norry MJ (eds). Special Publication 42. Geological Society: London; 313–345.
Tatsumi Y, Eggins S. 1995. *Subduction Zone Magmatism.* Blackwell: Cambridge, Massachusetts.
Tatsumi Y, Hamilton DL, Nesbitt RW. 1986. Chemical characteristics of fluid phase released from a subducted lithosphere and origin of arc magmas: evidence from high-pressure experiments and natural rocks. *Journal of Volcanology and Geothermal Research* **29**: 293–309.
Taylor SR, Gorton MP. 1977. Geochemical applications of spark-source mass spectrography, III. Element sensitivity, precision and accuracy. *Geochimica Cosmochimica Acta* **41**: 1375–1380.
Thorkelson DJ. 1985. Geology of the mid-Cretaceous volcanic units near Kingsvale, southwestern British Columbia. *Geological Survey of Canada Paper* **85–1B:** 333–339.
Thorkelson DJ. 1996. Subduction of diverging plates and the principal of slab window formation. *Tectonophysics* **225**: 47–63.
Thorkelson DJ, Rouse GE. 1989. Revised stratigraphic nomenclature and age determinations for mid-Cretaceous volcanic rocks in southwestern British Columbia. *Canadian Journal of Earth Sciences* **26**: 2016–2031.
Thorkelson DJ, Smith AD. 1989. Arc and intraplate volcanism in the Spences Bridge Group: implications for Cretaceous tectonics in the Canadian Cordillera. *Geology* **17**: 1093–1096.
Thorkelson DJ, Taylor RP. 1989. Cordilleran slab windows. *Geology* **17**: 833–836.
White WM, Patchett PJ. 1984. Hf-Nd-Sr isotopes and incompatible element abundances in island arcs: implications for magma origins and crust-mantle evolution. *Earth and Planetary Science Letters* **67**: 167–185.
Yogodzinski GM, Volynets ON, Kolosov AV, Seliverstov NI, Malvenkov VV. 1994. Magnesian andesites and the subduction component in a strongly calc-alkaline series at Piip volcano, far west Aleutians. *Journal of Petrology* **35**: 163–204.
Zindler A, Staudigel H, Batiza R. 1984. Isotope and trace element geochemistry of young Pacific seamounts: implications for the scale of upper mantle heterogeneity. *Earth and Planetary Science Letters* **70**: 175–195.

Scientific editing by Ron Pickerill.

